Journal of the European Ceramic Society **11** (1993) 445–453

Cyclic Fatigue Lifetime Predictions of Partially Stabilized Zirconia with Crack Resistance Curve Characteristics

Mark J. Hoffman, Werner Lentz, Michael V. Swain & Yiu-Wing Mai*

Centre for Advanced Materials Technology, Department of Mechanical Engineering, University of Sydney, Sydney, NSW 2006, Australia

(Received 23 December 1991; revised version received 8 September 1992; accepted 30 September 1992)

Abstract

Predictions of static and cyclic fatigue crack growth of indentation-initiated strength-limiting flaws in a Mg-PSZ material are compared with observations. The extent of environmental effects on cyclic loading lifetime prediction is determined by integrating the cyclic stress cycle following determination of crack growth parameters from static fatigue data. The effect of crack tip shielding as a result of the crack resistance curve is also included. The true cyclic fatigue effect is then determined. Crack growth dependence on the maximum stress intensity, K_{max}, and ΔK and possible mechanistic explanations of cyclic fatigue effect are also considered.

Die Vorhersage des Rißwachstums in Mg-PSZ bei statischer oder bei zyklischer Ermüdung, das an verzahnungsartigen, festigkeitsmindernden Fehlern eingeleitet wird, wird mit experimentellen Beobachtungen verglichen. Das Ausmaß umgebungsbedingter Einflüsse bei zyklischer Beanspruchung auf die Lebensdauervorhersage wurde bestimmt, indem über einen Spannungszyklus integriert wird. Die Parameter des Rißwachstums werden hierbei zuvor aus den Daten für den Fall statischer Beanspruchung gewonnen. Der Effekt der Abschirmung im Bereich der Rißspitze, wurde aus der Riß-Widerstandskurve bestimmt und mitberücksichtigt. Der tatsächliche Einfluß der zyklischen Ermüdung konnte damit bestimmt werden. Die Abhängigkeit des Rißwachstums von der maximalen Spannungsintensität K_{max} und von ΔK und mögliche mechanische Erklärungsansätze für den Effekt zyklischer Beanspruchung werden ebenfalls berücksichtigt.

Les auteurs comparent leurs observations expérimentales avec les prédictions de la croissance des fissures par fatigue statique et cyclique, dans le cas de défauts majeurs initiés par indentation dans un matériau Mg-PSZ. L'influence des effets d'environnement sur la prédiction de la durée de vie en mise en charge cyclique est déterminée en intégrant le cycle de contraintes cycliques, suivant la détermination des paramètres de croissance de fissure à partir des données de fatigue statique. L'effet de protection de front de fissure découlant de la courbe R est également inclus. L'effet de fatigue cyclique vrai est alors déterminé. La dépendance de la croissance de fissure vis-à-vis du maximum d'intensité de contrainte, K_{max}, ΔK et des explications possibles relevant de la mécanique sont également considérées pour expliquer l'effet de fatigue cyclique.

* To whom correspondence should be addressed.

1 Introduction

Ceramic materials have traditionally been thought of as being brittle in nature and exhibiting linear elastic behaviour. Observed strength degradation upon static loading has been associated with subcritical crack growth. Lifetime predictions for materials were based upon the cumulative time under static loading.[1,2]

Over the last decade there has been the development of a whole new class of toughened ceramics for structural applications. The toughening mechanisms used in these ceramics include:

—Fibre and whisker reinforcement
—Microcracking
—Crack deflection toughening
—Crack bridging
—Phase transformation toughening

Associated with these mechanisms there are energy dissipating processes about the crack tip which are a

Journal of the European Ceramic Society 0955-2219/93/$6.00 © 1993 Elsevier Science Publishers Ltd, England. Printed in Great Britain

consequence of non-linear stress–strain hysteretic behaviour. These mechanisms cause toughened ceramics to display crack resistance or *R*-curve behaviour.

Recent work has shown that these materials suffer mechanical cyclic degradation and hence a shortening of their predicted useful lifetimes under cyclic loading. This has been shown in a broad range of materials including aluminas,[3-5] zirconia ceramics[6-10] and silicon nitrides.[11] The typical means of verifying cyclic fatigue degradation has been to compare material lifetimes and crack growth rates under static versus cyclic loading.

Valid predictions of cyclic lifetimes have, however, been very difficult to make due to a lack of understanding of the cyclic degradation mechanism. There are a number of theories that have been recently proposed and supported by experimental evidence to explain a cyclic degradation mechanism. In the case of alumina, SEM observations revealed that cyclic loading caused the frictional degradation of bridging grains.[5] Subsequent models by the same workers[5,12] have proposed that frictional degradation is the dominant fatigue mechanism. Recent analytical work performed by Hu & Mai[13] and Hu *et al.*[14] show that a simple compliance measurement method may be used to determine the degradation of bridging stresses by frictional sliding in alumina ceramics. In the case of zirconia transformation toughened PSZ and TZP materials the toughening mechanisms are due to a volume expanding phase change rather than crack bridging. For these materials it is expected that the fatigue mechanism is more closely related to damage development around the crack tip. Two theories explaining cyclic degradation have been proposed in the case of zirconia ceramics:

(i) In-situ observations both at room temperature and elevated temperatures have been made of Mg-PSZ under cyclic loading conditions.[9] At lower temperatures, where material plasticity is greatest, the formation of slip lines has been observed at the crack tip. In a manner similar to that observed in metals, these slip lines have been seen to break down during subcritical cyclic loading, causing crack propagation.

(ii) In a series of experiments on Y-TZP cyclically loaded under uniaxial conditions[10,15] it has been proposed that during cyclic loading microcracks form throughout the bulk of the material, shown by a compliance change. These authors proposed that crack initiation occurs from some form of natural flaw either in the bulk or on the surface of the material. Under cyclic loading localized stresses about this natural flaw lead to the nucleation of microcracks which then coalesce, producing fracture and consequently a significant strength reduction under cyclic loading.

Studies have also been conducted on zirconia ceramics to observe fatigue in the small crack regime. Small cracks are defined as being of such a length that full crack tip shielding as a result of the toughening mechanism has not yet occurred, i.e. a plateau condition has not yet been reached in the *R*-curve. In the case of transforming materials, this refers to cracks that are shorter than five times the zone width. In the case of Mg-PSZ, tests under both static[16] and cyclic[17] loading have observed a negative sloping $\log(K_{applied})$ versus log(velocity) relationship, while crack tips have not yet a fully developed 'wake' zone behind them. In both cases material failure was observed to occur by a coalescence of small cracks.

The formation of microcracks following material loading has also been observed under high-resolution microscopy in three types of zirconia ceramic: ZTA, Mg-PSZ and Y-TZP.[18] The formation of these microcracks has been attributed to very large residual stresses as a result of martensitic transformation. Others argue that these large localized stresses may also be the result of elastic anisotropy.[19]

A number of difficulties exist with predicting the fatigue lifetimes under both static and cyclic loading for toughened ceramic materials. Traditionally fatigue crack growth has been expressed in terms of a power function. In the case of ceramic materials, however, this exponent is usually relatively large. The difficulty here is that small errors in the determination of the crack growth exponent or crack tip stress intensity lead to a very large difference in lifetime predictions.

A statistical approach to fatigue lifetime prediction has been developed by a number of authors[20-22] which incorporate a crack resistance curve effect by considering its effect on a Weibull strength distribution curve. It is noted that the growth of individual cracks in accordance with a slow crack growth equation is also considered in the work of Mai and coworkers.[20,21]

In the present paper the fatigue lifetime of Mg-PSZ is determined by integrating the velocity function of an indentation-initiated crack. The advantage of using an indentation crack is that unlike pre-existing flaws the crack dimensions can be predicted with reasonable accuracy to determine a crack tip stress intensity. In this study the crack was assumed to be of embedded semicircular shape.[23] Cyclic fatigue lifetimes are predicted as a result of environmental degradation determined from static

fatigue data. A sinh function,[12] which more appropriately incorporates upper and lower crack velocity thresholds, is used to represent static crack growth and is consequently integrated to determine cyclic fatigue lifetimes as a result of environmental influences. Unlike the more commonly used power function this function incorporates the thermally activated bond breaking processes of environmental degradation of the material in determining crack growth rates. Above the inert limit crack growth was unstable and independent of environmental effects and below the fatigue limit crack growth was zero. The effects of the material's crack resistance curve are also incorporated, with crack velocity being a function of the net crack-tip stress intensity factor.

In the case of both static and cyclic fatigue stable crack growth was deemed to occur between an inert limit and a fatigue limit. A true estimate of cyclic fatigue degradation can then be given independent of environmental effects.

2 Experimental

An explanation of the experimental work can be found in a previous paper.[7] However, a further description will be given here.

The material used was a TS-grade Mg-PSZ produced by Nilcra Ceramics containing 9·4 mol% MgO. The Young's modulus measured by flexural resonance method (Grindo Sonic) system was 207 GPa. All tests were undertaken under ambient conditions. The measured flexural strength was approximately 450 MPa. Indeed, in flexural experiments using strain gauges on the tensile surface and loaded on an Instron 1195 machine using a crosshead speed of 0·05 mm/min, it was observed that the onset of non-linearity occurred at about 350 MPa and there was little non-linearity up to 450 MPa. All the subsequent time-dependent strength experiments were conducted largely at stresses near or below the elastic limit.

Four-point bend specimens (with a 20 mm/30 mm inner to outer span ratio) were machined, ground and polished with 0·5–1 μm diamond pastes. X-Ray diffraction analysis showed that the monoclinic phase content was about 25% on the polished surface. Three Vickers indentations 5 mm apart were introduced on the polished surface of each specimen with a load of 20 kg held for 15 s. Prior to indentation the specimens were heated to 500°C and indented to reduce the phase transformation around the indentation and to enable the formation of larger radial cracks with minimal transformation about the tip. Observations using Nomarski interference showed that this was successful. Under these conditions the initial indentation cracks were approximately 400 μm in length.

Crack resistance curve experiments were performed on the bend specimens in an interrupted fashion so that the crack sizes could be measured using a replica technique at increasing loads. In this way the crack resistance (K_R) versus half-crack length (Δa) curves could be determined easily. In the replica technique an acetone-soluble cellulose-based replica material of 0·18–0·20 mm thickness was pressed against the indented/crack surface. It was allowed to dry for 7–10 min and the replica was peeled off and put on a microscope slide for measurement in an optical microscope. A size correction was made during this process to account for shrinkage of the polymer thin film upon drying.

Constant stress rate and constant applied stress experiments were carried out in the usual way. Constant applied amplitude cyclic experiments were studied using a piezoelectric resonance frequency testing machine at a frequency of approximately 220 Hz. The required mean stress was controlled mechanically by an adjustable turning screw and the stress range by an applied voltage to the piezoelectric crystal. The cyclic fatigue experiments were all conducted in tension–tension with a stress ratio (R) of 0·1.

Full experimental results can be seen in Figs 1–3,

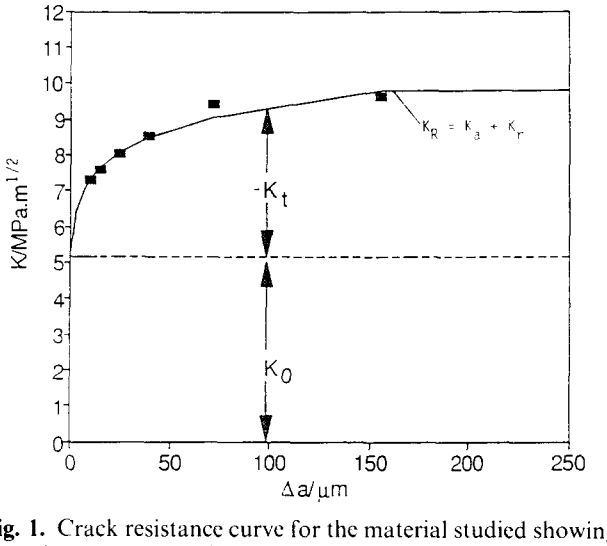

Fig. 1. Crack resistance curve for the material studied showing K_t and K_0 as used in the model. ■, Experimental data; ——, power law fit.

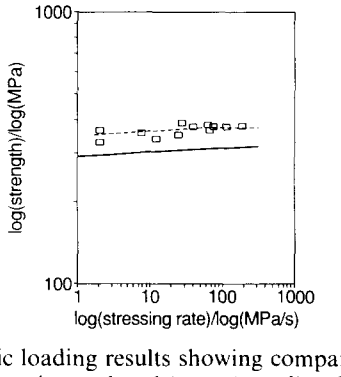

Fig. 2. Dynamic loading results showing comparison between (–⊟–) experimental and (——) predicted results.

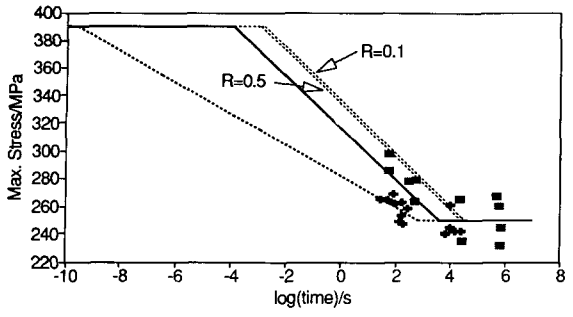

Fig. 3. Time-dependent fatigue results showing a comparison between predicted and experimental cyclic and static loading data. ■, Static experimental; +, cyclic experimental; ——, static; – – –, cyclic; – – –, predicted cyclic.

showing the crack-resistance curve and static and cyclic fatigue tests. In the case of all the fatigue tests cracks grew from initial lengths of 200 μm to approximately 600 μm, well in excess of the ceramic's grain size of 50 μm,

3 Crack Growth Predictions

3.1 Determination of K_* (crack-tip stress intensity)

Crack growth due either to monotonic or cyclic loading is essentially governed by the crack tip stress intensity, K_*. This is obtained by considering three components of stress intensity expressed as follows:

$$K_* = K_a + K_r + K_t \tag{1}$$

where K_a is the applied stress intensity factor due to the applied load. For this study an embedded circular crack is assumed giving:

$$K_a = \psi \sigma_a \sqrt{a + \Delta a} \tag{2}$$

where a is the initial crack length, Δa the crack extension and $\psi = 2/\pi^{1/2}$.[23]

K_r is the residual stress intensity factor which results from residual stresses which form around an indentation. This can be represented as:[23]

$$K_r = \S \left(\frac{E}{H}\right)^{1/2} \frac{P}{(a + \Delta a)^{3/2}} \tag{3}$$

For the Mg-PSZ used in this test, $\S = 0{\cdot}016$,[24] $E = 207$ GPa, $H = 9$ GPa for PSZ at 500°C, the indentation temperature,[25] and $P = 200$ N.

K_t is negative and represents the reduction in the crack-tip stress intensity factor due to toughening effects in the material.

3.2 Calculation of K_t

3.2.1 Analytical approaches

Extensive analytical work has been done in determining the toughening effect of transformation toughening (the recognized toughening mechanism in PSZ). The steady-state toughening effect can be quite accurately predicted from a prior knowledge of the zone shape and size as:[26]

$$K_t = \alpha e^T E f_v \sqrt{H_0} \tag{4}$$

where e^T is the transformation strain, E the Young's modulus, f_v the fraction of transforming material and H_0 the half-height of the transformed zone. α is a geometry factor which is equal to 0·22 for a hydrostatic stress profile and 0·25 for the semi-circular transformation zone profile observed in Mg-PSZ using Raman spectroscopy and optical interference imaging techniques.[27]

In the case of the present study, however, it is necessary to determine the toughening effect during the development of the wake zone behind the crack tip. A considerable amount of modelling work has been done to predict the toughening effect as the wake zone develops.[28–30] These models, however, have not been able to successfully explain the experimental R-curve profiles for a number of reasons. Firstly, experimental observations have revealed that the transformation zone shape does not follow a hydrostatic stress profile, as assumed in these models, but is more semicircular in shape.[31] The same study also found that the percentage of material transformed near the crack tip was always less than the possible maximum, i.e. f_v. Theoretical models have not considered this. Moreover, the determination of a toughening effect from observations of strains throughout the process zone concludes that, assuming a hydrostatic stress profile, the toughening effect determined accounts for only a part of the observed toughening in crack resistance curve tests.[32] A number of explanations exist for this, including the existence of non-hydrostatic and non-uniform strains in the process zone or that other toughening mechanisms may be present, e.g. micro-cracking, or that a significant component of shear strain is not relieved by twinning.[33]

3.2.2 Calculation of K_t from experimental data

Due to the factors mentioned previously, K_t for this study is determined from experimental data, namely the measured crack resistance curve, rather than using analytical methods. While this assumes a saturated toughening component for all crack growth, experience from previous work[12] has shown that this does not significantly affect the result and is a suitable estimation for the present model.

Initially an empirical fit of the R-curve data was made using the following equation:[23]

$$K_R = K_0 \left(\frac{a}{a_0}\right)^{\tau} \tag{5}$$

where a is the total crack length from the centre of the indent to the crack tip. A best fit was ob-

tained with $K_0 = 5{\cdot}14\,\text{MPa m}^{1/2}$, $a_0 = 0{\cdot}37\,\mu\text{m}$ and $\tau = 0{\cdot}108$.

A maximum value of $K_R = 9{\cdot}8\,\text{MPa}\sqrt{\text{m}}$ was set for all modelling work; this being the apparent value of the R-curve. The initial crack length was assumed to be $200{\cdot}37\,\mu\text{m}$ which was the initial crack length plus a_0 as determined in eqn (5).

From the R-curve K_t was determined as a function of the crack growth Δa:

$$-K_t = K_R - K_0 \tag{6}$$

as seen in Fig. 1, with K_0 being the intrinsic toughness of the material and $K_R = K_a + K_r$.

4 Crack Growth Velocity Predictions

Traditionally crack growth velocity is expressed in the form of some power law relation. Recently, however,[12] use has been made of a sinh function which has a number of advantages over the power law concept for the present study. The form of the equation is:

$$\left.\begin{aligned} v(G_*) &= v_0 \sinh\left[\frac{(G_* - 2\gamma_1}{\Gamma}\right] && (2\gamma_1 < G_* < 2\gamma_0) \\ v(G_*) &= 0 && (2\gamma_1 > G_*) \\ v(G_*) &= v_T && (2\gamma_0 < G_*) \end{aligned}\right\} \tag{7}$$

where G_* is the net crack-tip force and is equated by:

$$G_* = \frac{K_*^2}{E'} \tag{8}$$

where K_* is determined from eqn (1) and E' is the Young's modulus in plain strain.

The fracture surface energies are γ_1 and γ_0 in the presence of reactive and inert environments respectively. This system can be best represented as in Fig. 4. The two parameters v_0 and Γ represent the slope and intercepts of the crack growth profile respectively. v_T is the velocity at which a crack grows in an unstable condition when G_* exceeds the inert limit. It is set at 100 m/s for this model, being a very large velocity relative to that which occurs during stable

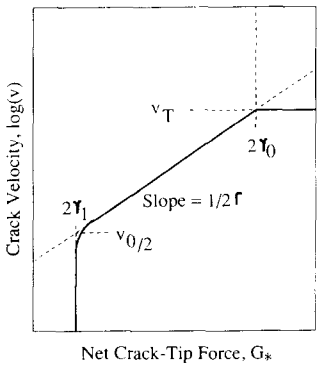

Fig. 4. Velocity function, $v(G_*)$, showing the effects of parameters used plotted logarithmically on the v-axis and linearly on the G_*-axis. (Courtesy of S. Lathabai & B. R. Lawn.)

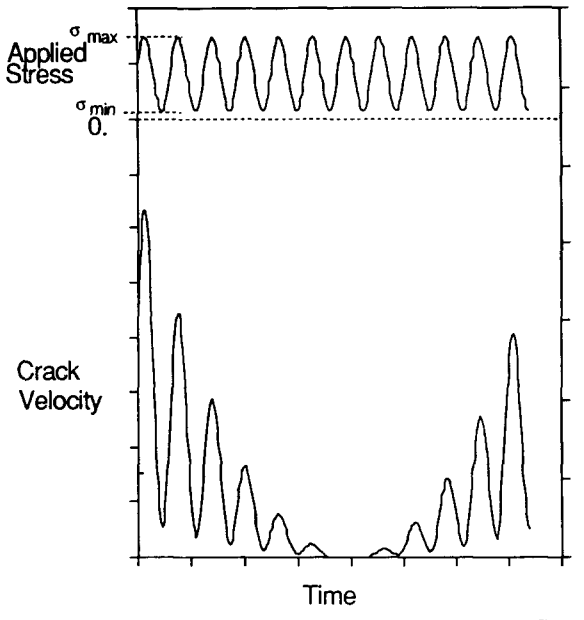

Fig. 5. A schematic comparison of the stress cycles' effect on crack growth velocity incorporating crack-tip shielding.

crack growth. The value of v_T will have very limited effect on the final result, for when $G_* > 2\gamma_0$ failure has already occurred. Below a certain net crack-tip force $2\gamma_1$ the crack will not progress, while above another net crack-tip force $2\gamma_0$ crack growth will be in an uncontrolled condition. In between these two regions crack growth will be stable and follows the sinh equation.

The major advantage of this equation over others is that it incorporates upper and lower bounds to fatigue crack growth plus the effects of crack-tip shielding, both of which are shown to exist with the material being observed in this paper. The advantages of this can be seen schematically in Fig. 5. The applied load is shown schematically in the form of a sine wave. Crack growth velocities vary not just as a function of the applied load but as a function also of the crack-tip shielding present, which is a function of crack growth. The effects of incorporating the crack growth limits can be seen in the centre of the crack growth velocity plot where crack growth ceases at the trough of the applied loading cycle as G_* falls below the fatigue threshold then continues again as applied load rises.

4.1 Determination of crack growth parameters

It is now necessary to determine the crack growth limiting energies, γ_1 and γ_0.

From the static loading tests a lower fatigue limit of 250 MPa can be observed in Fig. 3. This represents the occurrence of a situation at the crack tip in which the crack will not progress any further, this being the fatigue limit. An applied stress value of 250 MPa can then be substituted and into eqns (2) and (9) to obtain the lower curve in Fig. 6. The lowest point of this curve represents the minimum crack-tip force, $2\gamma_1$, below which crack growth will not occur.

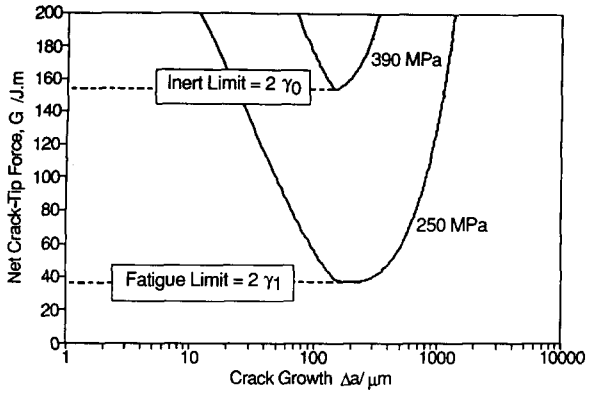

Fig. 6. Plot of $G_*(\Delta a)$ for the material used evaluated at the inert and fatigue limits as determined from experimental data.

Similarly an upper inert limit was found from the constant stressing rate data. In Fig. 2 an upper plateau of 390 MPa exists, representing the upper limit above which a crack will propagate in an uncontrolled state independent of environment. The principle here is that above a certain crack propagation rate the environment has limited effect upon bond breaking and subsequent unstable crack propagation. Hence there is an inert limit. The value of maximum crack-tip force is obtained in the same way as the lower limit by substituting the applied stress of 390 MPa into the crack-tip force equations. From this the upper curve in Fig. 6 is obtained. The lowest point on this curve is the inert limit crack-tip force equal to $2\gamma_0$. Thus

$$\gamma_0 = 76{\cdot}8\ \mathrm{J/m^2}$$

and

$$\gamma_1 = 18{\cdot}4\ \mathrm{J/m^2}$$

As the inert limit corresponded to an applied stress of 390 MPa a plateau in all time-to-failure modelling was obtained at that value, as seen in Fig. 3. At 390 MPa crack propagation was unstable and independent of both the loading method and history.

4.2 Application to static loading data and determination of v_0 and Γ

Static loading lifetime versus applied load curves are now obtained by integrating eqn (7) numerically employing a fourth-order Runge–Kutta system using time steps. The time step was varied depending upon crack growth velocity using an error checking routine. Failure was deemed to have occurred when crack-tip velocity equalled v_T, i.e. when net crack-tip force, G_*, exceeded $2\gamma_0$ and unstable crack growth occurred.

A series of applied loads were then employed to obtain a static fatigue curve. v_0 and Γ were then varied to obtain a best fit to the experimental data giving the curve in Fig. 3. Increasing v_0 caused the curve to move to the right, whereas increasing Γ caused the gradient of the line to decrease. A best fit was obtained with:

$$v_0 = 0{\cdot}15\ \mu\mathrm{m/s}$$

and

$$\Gamma = 0{\cdot}316\ \mathrm{J\,m^2}$$

4.3 Application to cyclic loading

The application of this system can now be made to cyclic loading. Applied load is administered in a cyclic form in the fashion of a time varying sine wave with:

$$\sigma = \frac{(1+R)}{2}\sigma_{max} + \frac{(1-R)}{2}\sigma_{max}\sin(2\pi\omega t) \qquad (9)$$

where the stress ratio R is defined by $\sigma_{min}/\sigma_{max}$. The loading cycle is represented in Fig. 5. The time step was held at a constant value depending upon cycling frequency (ω) with approximately 100 steps per cycle. Failure conditions were the same as in the static case.

As in the static loading case the velocity function is integrated to obtain time-to-failure versus maximum cyclic load plots as in Fig. 3. The stress ratio was set at 0·1 and frequency at 220 Hz. A stress ratio of 0·5 under the same frequency was also obtained for comparison.

4.4 Application to dynamic loading

The system was applied to the dynamic loading condition by applying stress in the form of:

$$\sigma = \dot{\sigma} t \qquad (10)$$

where $\dot{\sigma}$ is the stressing rate. Time steps were varied inversely with crack growth velocity and confirmed using an error checking routine at each step. The results in comparison with experimental data can be seen in Fig. 2.

5 Observations and Discussion

In the present study it can clearly be seen that the cyclic fatigue effect, i.e. the difference between the experimental and predicted values, increases significantly with increasing maximum cyclic stress. As all the tests were undertaken at a constant stress ratio increases in maximum cycling stress also corresponded to increases in ΔK. It is, therefore, not possible to discern the relative significance of ΔK and K_{max} in the present work.

There is little variation in the predicted cyclic fatigue lifetimes using two different stress ratios of 0·1 and 0·5. Experimental observations[8] have shown that by increasing the stressing ratio that cyclic fatigue lifetimes are increased, if only by a small

amount, relative to other materials. Predicted results, however, show that the opposite effect occurs, i.e. increasing the stressing ratio reduces the cyclic fatigue lifetime. This can easily be explained by considering Fig. 5. As K_{min} is increased the crack is subjected to a greater average K_* and hence crack growth velocities are higher and lifetimes shorter. The difference between predicted and experimental results, however, is added evidence of the effect of ΔK in cyclic fatigue degradation.

It was assumed in the present cyclic loading study that once G_* fell below a certain level no crack growth occurred. Significantly increased crack growth rates have been observed under tension–compression cycling. As mentioned earlier there is also a lower than may be expected variation between crack growth rates at higher and lower cyclic stress ratios. At higher stress ratios crack closure is considered a dominant crack-tip shielding mechanism.[33] However, the ocurrence of crack-tip closure results in compressive forces at the crack tip which may in fact enhance crack growth. A conclusion that may therefore be drawn is that some form of material breakdown occurs in cyclic loading as a result of compression at the crack tip, causing a net increase in crack growth rates. This may be a result of either applied compressive stresses, as in a tension–compression loading cycle, or crack-tip closure, which would be prevalent at high stress ratios.

As the cracks were initiated from indentations it was necessary to incorporate a residual stress intensity component into the crack-tip stress intensity. The resultant K_* can be seen in Fig. 7 for a static loading condition. K_* is high for very small crack extensions, essentially as a consequence of residual stresses resulting from the indentation. It then decreases quite rapidly as an outcome of both the steeply rising R-curve and decreasing residual stress intensity factor and then rises rather gradually. The effect of this on crack growth rates can be seen clearly in Fig. 8 which is for the case of a constant applied load of 280 MPa. Initially, at the loads used

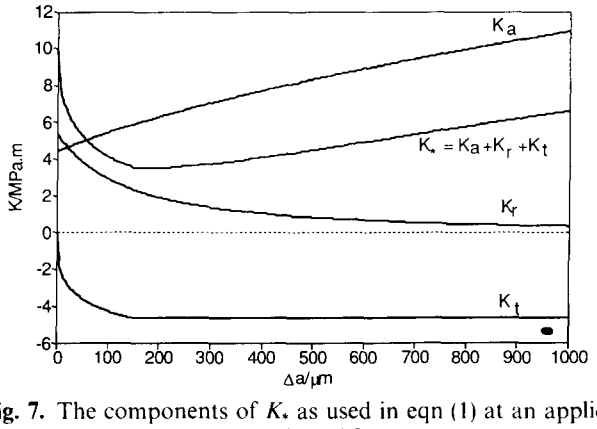

Fig. 7. The components of K_* as used in eqn (1) at an applied stress of 280 MPa.

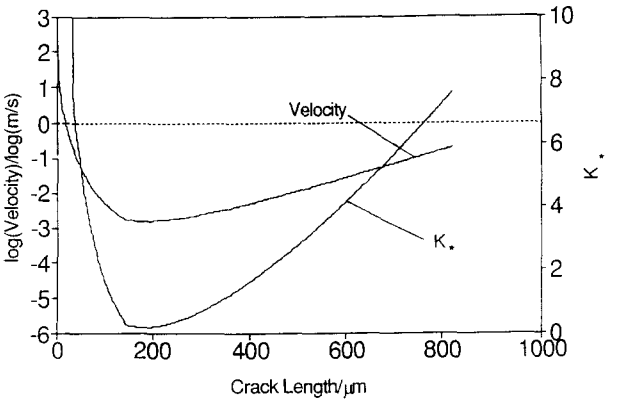

Fig. 8. $v(a+\Delta a)$ as determined from eqns (7) and (8) at an applied stress of 280 MPa.

in this study, the crack will grow in an unstable condition for a short initial stage of 15–100 μm depending upon the applied stress level. Stable crack growth will then occur until the crack-tip force exceeds the inert limit, usually between 600 and 1000 μm.

Figure 9 shows the relationship between crack growth rates and stress intensity factors K_* and K_a. It can be seen that while a negatively sloping curve occurs at lower levels of 'applied crack-tip stress intensity factor' due to the shielding factors mentioned previously, the crack growth versus actual crack-tip stress intensity (K_*) follows the expected pattern. This is analogous to the small crack effect observed in metal and ceramic materials.

Predicted times to failure are greater for cyclic loading than for static loading. As no damage mechanism was built into the model to account for cyclic load damage this was to be expected.

Figure 2 shows the failure strength versus stressing rate of dynamic fatigue results. While the model predicts somewhat lower strengths than those experimentally obtained an obvious correlation can be seen.

Traditionally, crack growth under cyclic loading in all materials has been assumed to be stress-range

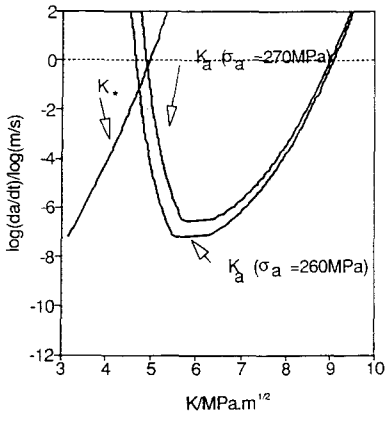

Fig. 9. Comparison of velocity as a function of K_a and K_* showing the negatively sloping K_a curve which is analogous to the small crack growth effect.

dependent and has been expressed according to:

$$\frac{da}{dN} = A(\Delta K)^n \tag{11}$$

In the case of zirconia ceramic materials a strong dependence on the maximum stress intensity has been observed,[15] which is somewhat consistent with the observation by the same authors that final failure appears to originate from pre-existing flaws. A loose dependence to ΔK^2 has also been observed for Mg-PSZ by some authors[6] and these observations have been combined to give:[15]

$$\frac{da}{dN} = B\left(\frac{K_{max}}{K_{IC}}\right)^n\left[\frac{\Delta K^2}{(\sigma^* E)}\right] \tag{12}$$

where σ^* is the characteristic stress for crack-tip plasticity at the crack tip, i.e. transformation stress or microcracking stress. Note that $\Delta K^2/(\sigma^* E)$ is essentially the crack-tip opening displacement (CTOD), indicating that the extent of crack-tip closure is significant, as proposed by other authors.[34]

6 Conclusions

It can be clearly seen that by integrating the stress cycle with incorporation of crack-tip shielding that cyclic fatigue is not a simple accumulation of environmental effects and that a distinct cyclic degradation mechanism is present.

The ΔK and the maximum stress intensity effect in cyclic fatigue can also be observed from the results. As the maximum cycling stress increases the variation between experimental cyclic fatigue lifetime and those obtained from static loading and integration of the stress cycle increases markedly. It was not possible from the present study to determine the independent significance of these two factors.

It is clear that to obtain accurate lifetime predictions a better knowledge of the cyclic fatigue mechanisms present in the material is essential. Very little has been done in this area especially to explain the mechanical fatigue mechanisms at the crack tip, except the work mentioned in the introduction. Once a damage mechanism is identified, whether due to degradation of crack wake shielding mechanisms or a reduction in the cyclic intrinsic toughness K_0 due to microcracking or shear/slip bands, it could be incorporated into the present model. This would be done by adding an extra term to eqn (1) which would effectively increase K_*. More experimental work is necessary, however, before necessary assumptions may be made to accurately predict cyclic fatigue lifetimes.

Acknowledgements

The authors wish to thank the Australian Research Council and the GIRD NMTC programme for the support of this work. M.J.H. also thanks ICI Advanced Ceramics and DEET for the Postgraduate Research with Industry Award tenable at the University of Sydney.

References

1. Evans, A. G. & Fuller, E. R., Crack propagation in ceramic materials under cyclic loading conditions. *Metallurg. Trans.*, **50** (1974) 27–33.
2. Evans, A. G., Fatigue in Ceramics. *Int. J. Fract.*, **16** (1980) 485–98.
3. Reece, M. J., Guiu, F. & Sammur, M. F. R., Cyclic fatigue crack propagation in alumina under direct tension–compression loading. *J. Amer. Ceram. Soc.*, **72**(7) (1989) 348–52.
4. Ewart, L. & Suresh, S., Crack propagation in ceramics under cyclic loads. *J. Mat. Sci.*, **22**(4) (1987) 1173–92.
5. Lathabai, S., Rödel, J. & Lawn, B. R., Cyclic fatigue from frictional degradation at bridging grains in alumina. *J. Amer. Ceram. Soc.*, **74**(6) (1991) 1340–8.
6. Dauskardt, R. H., Marshall, D. B. & Ritchie, R. O., Cyclic fatigue crack propagation in magnesia-partially-stabilized zirconia ceramics. *J. Amer. Ceram. Soc.*, **73**(4) (1990) 893–903.
7. Lentz, W., Mai, Y.-W., Swain, M. V. & Cotterell, B., Time dependent strength behaviour of Mg-PSZ with *R*-curve characteristics. In *Proceedings Austceram. 90*, Transtech Publications, Aedermannsdorf, Switzerland, 1990, pp. 750–3.
8. Swain, M. V. & Zelizko, V., Comparison of static and cyclic fatigue on Mg-PSZ alloys. *Adv. Ceram.*, **24** (1988) 595–606.
9. Davidson, D., Campbell, J. B. & Lankford, J., Fatigue crack growth through partially stabilized zirconia at ambient and elevated temperatures. *Acta Metall. Mater.*, **39**(6) (1991) 1319–30.
10. Shih-Yu Liu & I-Wei Chen, Fatigue of yttria-stabilized zirconia: I. Fatigue damage, fracture origins, and lifetime prediction. *J. Amer. Ceram. Soc.*, **74**(6) (1991) 1197–205.
11. Masuda, M., Soma, T., Matsui, M. & Oda, I., Cyclic fatigue of sintered silicon nitride. *J. Eur. Ceram. Soc.*, **6**(4) (1990) 253–8.
12. Lathabai, S., Mai, Y.-W. & Lawn, B. R., Cyclic fatigue behaviour of an alumina ceramic with crack resistance characteristics. *J. Amer. Ceram. Soc.*, **72**(9) (1989) 1760–3.
13. Hu, X.-Z. & Mai, Y.-W., Crack bridging analysis for alumina ceramics under monotonic and cyclic loading. *J. Amer. Ceram. Soc.*, **75**(4) (1992) 848–53.
14. Hu, X.-Z., Mai, Y.-W. & Lathabai. S., Compliance analysis of a bridged crack under monotonic and cyclic loading. *J. Eur. Ceram. Soc.*, **9** (1992) 213–17.
15. Shih-Yu Liu & I-Wei Chen, Fatigue of yttria-stabilized zirconia: II. Crack propagation, fatigue striations and short-crack behaviour. *J. Amer. Ceram. Soc.*, **74**(6) (1991) 1206–16.
16. Jensen, D., Zelizko, V. & Swain, M. V., Small flaw static fatigue crack growth in Mg-PSZ. *J. Mater. Sci. Lett.*, **8** (1983) 1154.
17. Steffen, A. A., Dauskardt, R. H. & Ritchie, R. O., Cyclic fatigue life and crack-growth behaviour of microstructurally small cracks in magnesia-partially-stabilized zirconia ceramics. *J. Amer. Ceram. Soc.*, **74**(6) (1991) 1259–68.
18. Heuer, A. H., Ruhle, M. & Marshall, D. B., On the thermoelastic martensitic transformation in tetragonal zirconia. *J. Amer. Ceram. Soc.*, **73**(4) (1990) 1084–93.

19. Marshall, D. B. & Swain, M. V., Crack resistance curves in magnesia-partially stabilized zirconia. *J. Amer. Ceram. Soc.*, **71**(6) (1988) 399–407.
20. Duan, K., Mai, Y.-W. Cotterell, B., A statistical fracture mechanics analysis of time-dependent strength behaviour of partially stabilized zirconia. *J. Mater. Sci.*, **23** (1988) 3671–7.
21. Hu, X.-Z., Mai, Y.-W. & Cotterell, A statistical theory of time-dependent fracture for brittle materials. *Phil. Mag.*, **58** (1988) 292–324.
22. Fett, T., Martin, G., Munz, D. & Thun, G., Determination of da/dN–ΔK_I-curves for small cracks in alumina in alternating bending tests. *J. Mater. Sci.* (in press).
23. Cook, R. F. & Clarke, D. R., Fracture stability, *R*-curves and strength variability. *Acta Metall.*, **36**(3) (1988) 555–62.
24. Antis, G. R., Chantikul, P., Lawn, B. R. & Marshall, D. B., A critical evaluation of indentation techniques for measuring fracture toughness: I. Direct crack measurements. *J. Amer. Ceram. Soc.*, **64**(9) (1981) 533–8.
25. Hannink, R. H. J. & Swain, M. V., Indentation studies of zirconia ceramics. In *Proceedings Austceram. 1984*, Australian Ceramic Society, Melbourne, Australia, pp. 137–43.
26. Marshall, D. B., Drory, M. & Evans, A. G., Transformation toughening in ceramics. *Fract. Mech. Ceram.*, **6** (1983) 289.
27. McMeeking, R. M. & Evans, A. G., Mechanics of transformation toughening in brittle materials. *J. Amer. Ceram. Soc.*, **65**(5) (1982) 242–6.
28. Stump, D. M. & Budiansky, B., Finite cracks in transformation-toughened ceramics. *Acta Metall.*, **37**(12) (1989) 3297–304.
29. Budiansky, B., Hutchinson, J. W. & Lambropoulos, J. C., Continuum theory of dilatant transformation toughening in ceramics. *Int. J. Solids Struct.*, **19** (1983) 337.
30. Duan, K., Cotterell, B. & Mai, Y.-W., Static fatigue in dilatant zone toughened ceramics. Presented at *23rd National Symposium on Fracture Mechanics*, 18 20 June 1991. College Station, Texas, USA.
31. Marshall, D. B., Shaw, M. C., Dauskardt, R. H., Ritchie, R. O., Readley, M. J. & Heuer, A. H., Crack-tip transformation zones in toughened zirconia. *J. Amer. Ceram. Soc.*, **73**(9) (1990) 2659–66.
32. Dadkhah, M. S., Marshall, D. B., Morris, W L., & Cox, B. N., Direct measurement of transformation zone strains in toughened zirconia. *J. Amer. Ceram. Soc.*, **74** (1990) 2939.
33. Stump, D. M., The role of shear stresses and shear strains in transformation toughening. *Phil. Mag.*, **64** (1991) 879–902.
34. Ritchie, R. O., Mechanisms of fatigue crack propagation in metals, ceramics and composites: role of crack tip shielding. *Mater. Sci. Eng.*, **A103** (1988) 15–28.